JOURNAL OF SPACECRAFT AND ROCKETS
Vol. 50, No. 4, July–August 2013

Explosion Hazard from a Propellant-Tank Breach in Liquid Hydrogen-Oxygen Rockets

Viatcheslav Osipov,* Cyrill Muratov,† Halyna Hafiychuk,‡ Ekaterina Ponizovskaya-Devine,‡
Vadim Smelyanskiy,§ Donovan Mathias,¶ Scott Lawrence,¶ and Mary Werkheiser**
NASA Ames Research Center, Moffett Field, California 94035

DOI: 10.2514/1.A32277

An engineering risk assessment of the conditions for massive explosions of cryogenic liquid hydrogen-oxygen rockets during launch accidents is presented. The assessment is based on the analysis of the data of purposeful rupture experiments with liquid oxygen and hydrogen tanks and on an interpretation of these data via analytical semiquantitative estimates and numerical simulations of simplified models for the whole range of the physical phenomena governing the outcome of a propellant-tank breach. The following sequence of events is reconstructed: rupture of fuel tanks, escape of the fluids from the ruptured tanks, liquid film boiling, fragmentation of liquid flow, formation of aerosol oxygen and hydrogen clouds, mixing of the clouds, droplet evaporation, self-ignition of the aerosol clouds, and aerosol combustion. The power of the explosion is determined by a small fraction of the escaped cryogens that become well mixed within the aerosol cloud during the delay time between rupture and ignition. Several scenarios of cavitation-induced self-ignition of the cryogenic hydrogen/oxygen mixture are discussed. The explosion parameters in a particular accident are expected to be highly varied and unpredictable due to randomness of the processes of formation, mixing, and ignition of oxygen and hydrogen clouds. Under certain conditions rocket accidents may result in very strong explosions with blast pressures from a few atm up to 100 atm. The most dangerous situations and the foreseeable risks for space missions are uncovered.

Nomenclature

C	=	specific heat at constant pressure, J/kg/K
C_d	=	drag coefficient
C_i	=	concentration of ith component, mol/m^3
κ	=	thermal conductivity, W/m/K
L	=	size of mixed H2/Ox clouds, m
L_D	=	thermo-diffusion length, m
M_i	=	molar mass of the ith component, kg
P	=	pressure, Pa
R_i	=	gas constant for the ith species, J/kg/K
R_b	=	bubble radius, m
R_{burn}	=	burning rate, mol/s/m^3
S	=	cross-sectional area, m^2
T	=	temperature, K
β	=	accommodation coefficient
μ	=	dynamic viscosity, Pa · s
ρ	=	mass density, kg/m^3
σ	=	surface tension, N/m
τ	=	characteristic time, s

Subscripts

cj	=	Chapman-Jouguet point
evap	=	evaporation
g	=	gas
h	=	hole
H2	=	hydrogen
ign	=	ignition
L	=	liquid
max	=	maximum
mix	=	mixture
Ox	=	oxygen
v	=	vapor
0	=	initial state

Received 9 November 2011; revision received 24 December 2012; accepted for publication 11 January 2013; published online 25 June 2013.

*Senior Research Scientist, MCT Inc., Applied Physics Group, Intelligent Systems Division.

†Associate Professor, Department of Mathematical Sciences, New Jersey Institute of Technology, Newark, NJ 07102.

‡Research Scientist, SGT, Inc., Applied Physics Group, Intelligent Systems Division.

§Principal Scientist, Exploration Technology Directorate, Applied Physics Group Lead, Intelligent Systems Division.

¶Aerospace Engineer, Supercomputing Division, MS 258-1.

**Engineering Project Manager, NASA Marshall Space Flight Center, Huntsville, AL 35812.

I. Introduction

A MASSIVE explosion of a liquid-propellant rocket in the course of an accident can lead to a truly catastrophic event. This point was amply demonstrated by the *Challenger* disaster of 1986 and was again brought to mind by a recent failure of the Russian Progress rocket, which led to an explosion that rattled windows nearly 100 km away from the crash site. The *Challenger* disaster provoked studies of various risks that can lead to similar catastrophic events related to the use of cryogenic hydrogen/oxygen (H2/Ox) propellants. As was established by the *Challenger* investigation, the original source of the disaster was freezing of the O-ring in the lower section of the left solid booster and formation of a gas leak through the O-ring [1–3]. This leak developed into a strong jet of hot gases from the booster and caused separation of the lower dome from the rest of the H2 tank (Fig. 1, "original failure"). As a result the tank began to accelerate upward under the action of the gas pressure inside the tank. The accelerating liquid-hydrogen (LH2) tank broke the liquid-oxygen (LOx) feed line in the intertank space and then the LOx tank's bottom dome. The resulting LOx stream from the broken LOx feed line was injected into the intertank space mixing with the gaseous-hydrogen (GH2) jet from the rupture of the H2 tank top dome and then self-ignited near the intertank section (Fig. 1, "first fire").

The *Challenger* disaster represents only one possible scenario of the sequence of catastrophic events involving potentially explosive cryogenic propellants such as LH2 and LOx. Another scenario has to

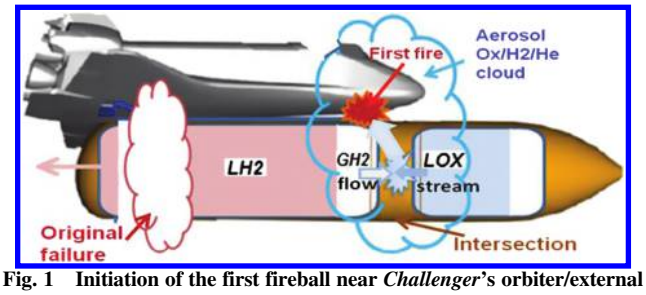

Fig. 1 Initiation of the first fireball near *Challenger*'s orbiter/external tank forward attachment.

do with an uncontained failure of the first stage of an LH2/LOx liquid rocket shortly after launch whereby the fully loaded tanks of the second and third stages come crashing down to the ground, violently releasing their entire content into the air [4]. To assess the power of the ensuing explosion, many factors determined by the whole range of physical processes leading to the explosion have to be taken into consideration. In a situation where the LH2 tank hits the ground first, the following sequence of events takes place: first, as the LH2 storage tank disintegrates upon impact, LH2 is ejected from the rocket onto the ground; second, the resulting splash of rapidly evaporating LH2 produces GH2 and a spray of LH2 droplets in the air that are expanding from the impact location; third, after some delay the rupture of the LOx tank leads to ejection of LOx and the formation of a LOx spray into the GH2-rich area. Direct contact between LH2 and LOx streams is known experimentally to lead to self-ignition of hydrogen/oxygen mixtures [5]. The energy released by the H2/Ox combustion then further vaporizes the liquid propellants, increasing their mass in the gas phase and making them available for further reaction. This positive feedback mechanism may produce a powerful explosion.

The analysis of the underlying physical processes and catastrophic risks associated with the use of cryogenic propellants in rocket engines presents a number of puzzles. Up until now, the most baffling event in the sequence leading to the Orbiter's disintegration in the *Challenger* disaster has been the initial formation of flames near the intertank section and not near the engine nozzles [1–3]. It is quite surprising that the mixture of cryogenic GH2 and LOx/GOx (gaseous oxygen) self-ignited near the intertank region (Fig. 1, "first fire"), considering the fact that LOx is stored at a very low temperature of about 90 K and LH2 is stored at an even lower temperature of only about 20 K in the tanks. At the same time, the self-ignition temperature for GH2/GOx mixtures at atmospheric pressure is about 850 K [6]. Similarly, the power of the explosion following an uncontained first stage failure should depend on the degree of H2 and Ox mixing before the ignition occurs. Clearly, only the (possibly small) region in which the propellants are well mixed can participate in the chemical reaction. Furthermore, the fraction of well mixed propellants sensitively depends on the time delay between the propellant release and the moment of ignition. The character of the explosion (a strong blast or a weak deflagration) should also strongly depend on the initial density and temperature of the mixed propellants.

To develop a better understanding of the magnitude and the character of explosions resulting from a breach of LH2/LOx tanks, and to clarify the important questions about cryogenic H2/Ox explosion mechanisms, Hydrogen-Oxygen vertical-impact (HOVI) tests were carried out at the NASA Johnson Space Center's White Sands test facility [7]. These tests simulated fully loaded rocket stages falling onto the ground in the course of a launch accident with tank configurations similar to those in a launch vehicle. The results of the HOVI tests showed some surprising characteristics of the explosions involving cryogenic LH2/LOx propellants. In particular, in each test the propellant mixtures that formed always self-ignited despite careful removal of all possible external sources of ignition and despite very low temperatures in the mixture. Furthermore, the combustion wave that formed in most of the HOVI tests was neither a deflagration nor a detonation wave and had unusual characteristics. Most importantly, although the majority of the explosions produced relatively weak blasts, some of the tests produced very powerful blasts.

This paper aims to characterize the conditions and risks of strong explosions in LH2/LOx cryogenic rockets following a launch accident based on the data obtained in the HOVI tests. It is, however, impossible to achieve this aim without considering the totality of the complex physical phenomena occurring in the course of an accident, often taking place within the "integrated vehicle environment." Therefore, the analysis of this paper required developing diverse yet interconnected physical models, ranging from a mechanical model of propellant-tank rupture to a model of shock formation at ground impact, a model describing the escape of fluids from the ruptured tanks, a model of flow fragmentation and Leidenfrost effect for the cryogenic droplets evaporating at the contact with the ground, etc. In fact, some of the physical phenomena involved are very poorly understood. Inevitably, when dealing with such a wide range of physical processes, some gross modeling simplifications are necessary. The approach adopted in this paper is to study these extremely complex physical processes using simplified physics-based models that may allow us to obtain the correct order-of-magnitude estimates of the parameters of the considered processes that are most significant for establishing a general qualitative picture of the accident. The goal of the paper was, therefore, not to undertake detailed analyses of each fragment of this extremely complex problem but rather to reconstruct a consistent picture of the accident as a whole and to draw conclusions based on our interpretation of the HOVI tests about the characteristics and the risk factors for powerful explosions during accidents involving cryogenic liquid-propellant rockets.

II. Summary of the Hydrogen-Oxygen Vertical-Impact Test Data

To characterize the mixing and explosion processes of LH2/LOx and other propellant combinations NASA performed an extensive series of tests at its White Sands test facility over a 10-year period during the 1990s [7]. Among those tests the HOVI tests served to obtain explosion data typical of a catastrophic failure of an LH2/LOx-based launch vehicle. In this paper we only discuss the results from those tests that are the most representative of a particular scenario to highlight the underlying physics.

In the HOVI tests several types of tank configurations (Fig. 2) were hoisted to the top of a 76-m-tall drop tower and then allowed to fall to the ground. The impact velocity was $30 \div 35$ m/s. The tank configurations were similar to those in the external tank of the space shuttle and other launch vehicles. In all the HOVI tests the LOx tank was placed above the LH2 tank. The tanks were made of an aluminum alloy and insulated with 0.5-inch-thick polyurethane foam. In the first configuration group (Fig. 2a, HOVI tests 13 and 14; Fig. 2b, HOVI tests 9 and 10), the LH2 and LOx tanks were joined, whereas in the second configuration group (Fig. 2c, HOVI tests 2 and 5) the LOx tank alone was dropped from the tower and collided with the LH2 tank resting on the ground. These groups also differed by the location of the rupture devices. In the first group a rupture device was placed underneath each tank (Figs. 2a and 2b), whereas in the second group a single rupture device was placed between the tanks (Fig. 2c). The LH2 (LOx) tanks in HOVI tests 13 and 14 had diameter $D_t = 0.94$ m, heights $H_t = 3.84\,(1.42)$ m, total volumes $V_t = 2.396\,(0.817)$ m^3, and ullage gas volumes $V_{g0} = 0.553\,(0.081)$ m^3. The pressures in the tanks were $p_{H2} = 1.43$ atm and $p_{\mathrm{Ox}} = 3.15$ atm. The double tanks in HOVI tests 9 and 10 had each LH2 (LOx) tank with $D_t = 0.46$ m, $H_t = 1.78\,(0.71)$ m, total volumes $V_t = 0.273\,(0.095)$ m^3, ullage gas volumes $V_{g0} = 0.037\,(0.018)$ m^3, and pressures $p_{\mathrm{H2}} = 1.43$ atm and $p_{\mathrm{Ox}} = 3.42$ atm. The LH2 (LOx) tanks in HOVI tests 2 and 5 had $D_t = 0.58$ m, $H_t = 2.24\,(0.86)$ m, total volumes $V_t = 0.545\,(0.185)$ m^3, ullage gas volumes $V_{g0} = 0.016\,(0.019)$ m^3, and pressures $p_{\mathrm{H2}} = 1.43$ atm and $p_{\mathrm{Ox}} = 3.38$ atm (HOVI test 2) and $p_{\mathrm{Ox}} = 5$ atm (HOVI test 5). Other parameters of these tests are given in Table 1.

The schematics of the instrumentation at the HOVI test site are presented in Fig. 3. Piezoelectric transducers were used to record

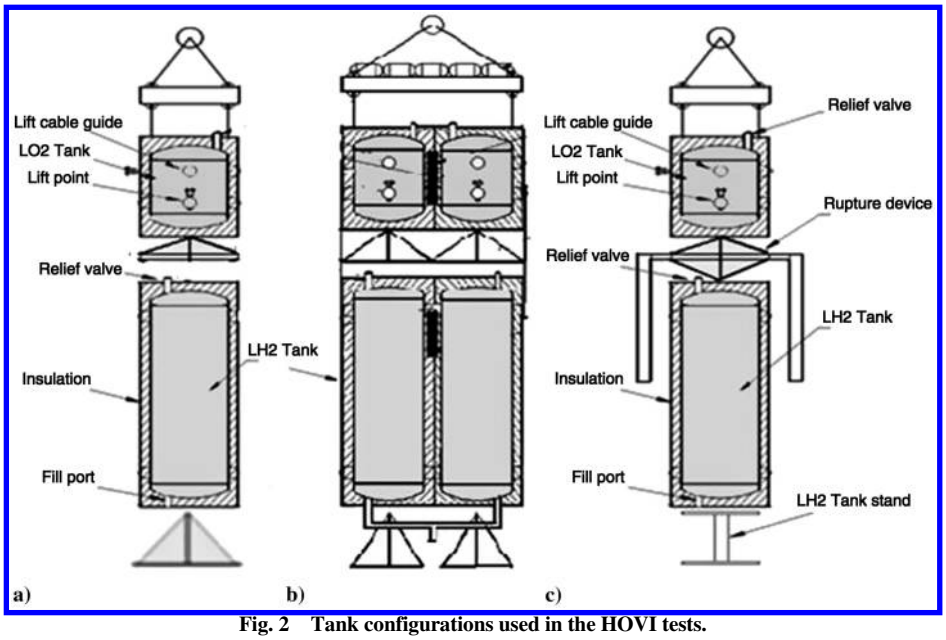

Fig. 2 Tank configurations used in the HOVI tests.

pressures at different locations around ground zero (a concrete pad). Pressure-sensor arrays at 10 distances from ground zero were located along legs 1, 2, and 3 within the test area (Fig. 3). In addition, a 9-m-long elevated gauge line (EGL) with five pairs of pressure gauges made a 20-deg angle with the ground. The data from gauges at ground level and those from the EGL did not differ significantly from each other. Depending on the distance from ground zero (Fig. 3) four types of transducers were used: pressure range 0–5000 psi in ring 1 (1.2 m); 0–1000 psi in ring 2 (1.7 m); 0–500 psi in ring 3 (2.5 m); and 0–100 psi in rings 4–10 beyond the radius of 3.6 m, respectively. Sensors with pressure range 0–100 psi were also used for the EGL. In addition, there were three camera bunkers with standard VHS video cameras (30 fps) and two film cameras, one 10,000-fps camera (Hycam) and one 500-fps camera (Locam). The explosions occurred in roughly hemispherical cryogenic clouds escaping from the ruptured tanks at or near the ground level and were approximately radially symmetric.

Both the HOVI tests and the LH2/LOx pan (Dewar) tests performed at the site earlier demonstrated that rapid ignition of LH2/LOx mixtures always occurred spontaneously and was not due to external heat sources.

According to the HOVI tests, however, LH2 alone is not prone to self-ignition because in all the HOVI tests ignition never occurred after an LH2 spill but before LOx was released. The HOVI test data also showed that an LH2 spill alone is not likely to self-ignite quickly because in every HOVI test in which a ground cloud of LH2 formed after rupture of the LH2 tank bottom the ground H2 cloud did not ignite until LOx was released. The HOVI test data confirmed the tendency of prompt LH2/LOx mixture self-ignition because each HOVI test ignited without external assistance within tens of

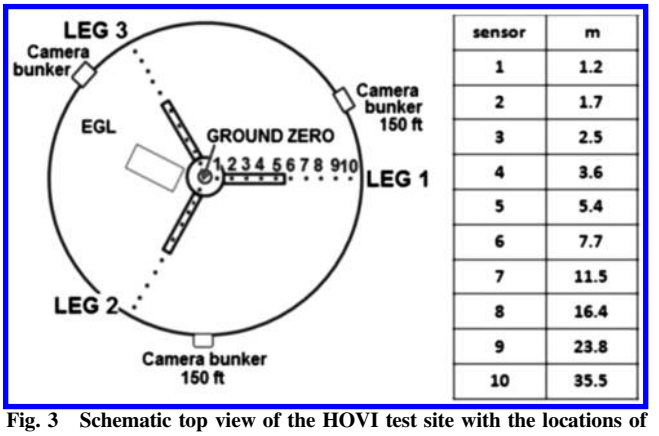

sensor	m
1	1.2
2	1.7
3	2.5
4	3.6
5	5.4
6	7.7
7	11.5
8	16.4
9	23.8
10	35.5

Fig. 3 Schematic top view of the HOVI test site with the locations of pressure sensors.

milliseconds following impact as soon as the cryogenic H2 and Ox came into contact. The modes of the tank rupture in each group of the HOVI tests are shown in Fig. 4. In the first group (HOVI tests 9, 13, and 14), upon impact the bottom dome of the LH2 tank is ruptured first, ejecting a stream of LH2 into the ground.

After some delay the bottom dome of the LOx tank is then ruptured ejecting a stream of LOx colliding with the top of the LH2 tank. Both the LH2 and the LOx streams are fragmented into partially evaporating liquid droplets. The resulting H2 aerosol cloud appears at the ground level, while the Ox aerosol cloud appears in the region between the tanks after delay time $t_{\text{delay}} \sim (20 \div 40)$ ms (Fig. 4, left). These aerosol clouds partly mix, and an explosion is observed at time

Table 1 Summary of the main quantitative characteristics of the HOVI test data

HOVI test (group)	Total LH2 mass in the tanks, kg	Total LOx mass in the tanks, kg	Yield, %	Dimensions (horizontal half width x height) of H2/Ox aerosol cloud at ignition, m	Time delay before the explosion, ms	Maximum pressure, atm	Pressure wave speed, m/s	Pressure wave duration, ms
13 (1)	129	840	~3.3	4.1×2	~90	$3.3 \div 4.2$	$\approx 740 \div 920$	≈ 3.5
14 (1)	154	864	~5.7	3.2×3.2	~130	$3.4 \div 4.3$	$\approx 620 \div 925$	≈ 5
9 (1), double tanks	$33 \times 2 = 66$	$176 \times 2 = 352$	~36	6×4.6	~200	$80 \div 110$	$2625 \div 2966$	≈ 0.7
2 (2)	37	189	~3.2	1×1.4	~20	$3.2 \div 5.4$	≈ 780	≈ 3.4
5 (2)	36	185	~2.8	— —	<1	$2.5 \div 3$	≈ 660	≈ 4.0
10 (2), double tanks	$36 \times 2 = 72$	$186 \times 2 = 372$	~2.7	— —	<1	$1.2 \div 1.4$	≈ 600	≈ 4.0

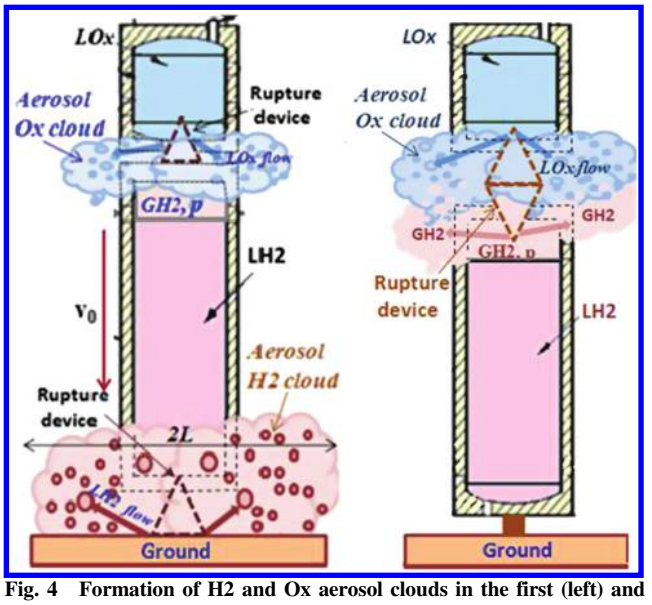

Fig. 4 Formation of H2 and Ox aerosol clouds in the first (left) and second (right) HOVI test groups.

$t_{\text{blast}} \sim (60 \div 100)$ ms following the impact (see Table 1). This time roughly coincides with the travel time of the released LOx fragments to hit the ground. The explosions are characterized by the pressure-sensor data presented in Fig. 5. Figure 5 (top, left) shows two representative time traces from the pressure sensors located close to ground zero during HOVI test 13. Specifically, they show pressure versus time for the sensors on leg 1 at distances 1.2 m (4 ft) and 1.7 m (5.8 ft) from ground zero (Fig. 3), respectively. The maximum pressure recorded by all sensors is $p_{\max} = 4.2$ atm, and the blast wave speed recorded between these sensors is $v = 740 \div 825$ m/s. Similar results were obtained in other tests in this group, such as HOVI test 14, except for HOVI test 9. Representative sensor data for HOVI test 9 presented in Fig. 5 (top, right) show that the maximum pressure recorded was $p_{\max} = 110$ atm and the blast speed was $v = 2625 \div 2966$ m/s, which is considerably higher than in all other tests in this group.

In the second group of tests (HOVI tests 2 and 5) a LOx tank was dropped onto an LH2 tank resting on the ground with rupture of the bottom dome of the LOx tank and the top dome of the LH2 tank occurring almost simultaneously upon impact (Fig. 4, right). As a result very little (20 ms for HOVI test 2) or no delay between the impact and ignition was observed. In HOVI test 2 the rupture device was slightly elevated relative to the LH2 tank top. As a consequence a small LOx cloud (about 1-m radius) was observed at the moment of ignition. The power and the maximum recorded pressures in these explosions were lower than in the first group, whereas other characteristics such as the blast wave speed were similar (see Fig. 5 bottom and Table 1).

III. Physical Interpretation of the Hydrogen-Oxygen Vertical-Impact Test Data

The explosion data obtained in the HOVI tests present significant difficulties in terms of their interpretation because they do not readily fall into the standard combustion/explosion scenarios. Specifically, in all tests except one the observed fireballs exhibited flame front speeds and pressures that are consistent with neither deflagration nor detonation waves forming in unconfined GH2/GOx mixtures under standard conditions. In fact, our analysis shows that the data also do not agree with the deflagration and detonation wave characteristics under cryogenic conditions of the GH2/GOx clouds. Therefore, the aerosol nature of these clouds must be taken into consideration. This poses a further set of questions such as what are the characteristic sizes and velocities of the liquid droplets in those clouds and how these droplets contribute towards the flame front speed. A separate question is how the observed flames are initiated in the first place. A consistent physics-based interpretation of the observed phenomena is provided next.

A. Detonation and Deflagration Waves in Unconfined Gaseous GH2/GOx/GN2 Mixtures

First, to compare the experimental data from the HOVI tests with the conventional scenarios, the detonation and deflagration characteristics of cryogenic GH2/GOx/GN2 mixture explosions are analyzed as functions of mixture temperature and composition. Detonation is supersonic combustion accompanied by a strong shock

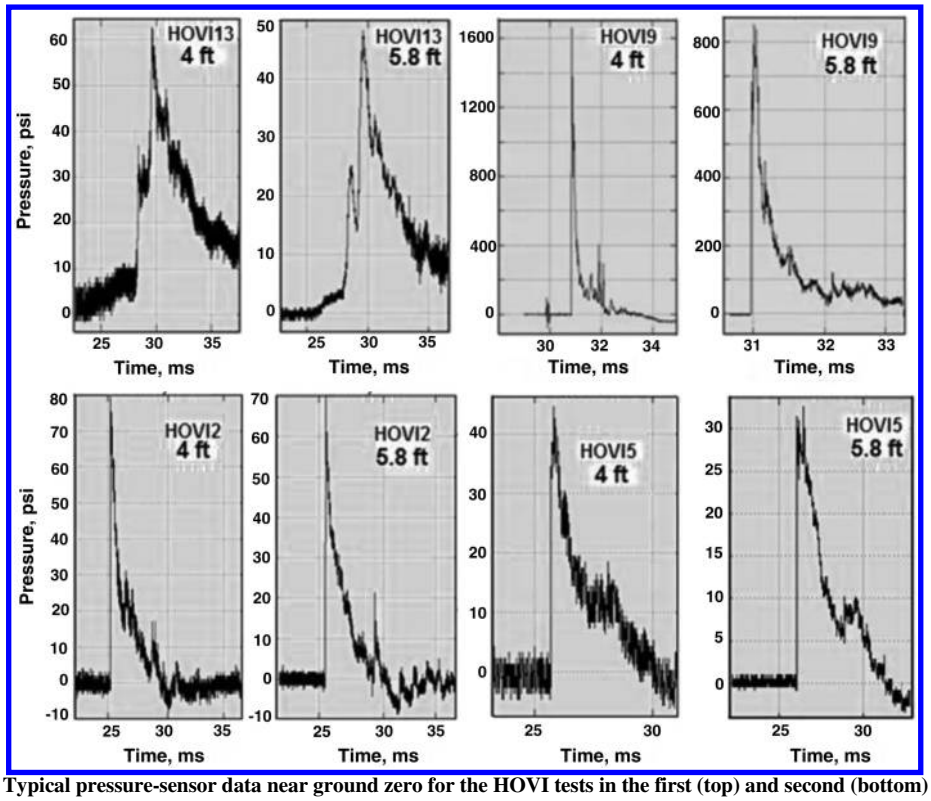

Fig. 5 Typical pressure-sensor data near ground zero for the HOVI tests in the first (top) and second (bottom) groups.

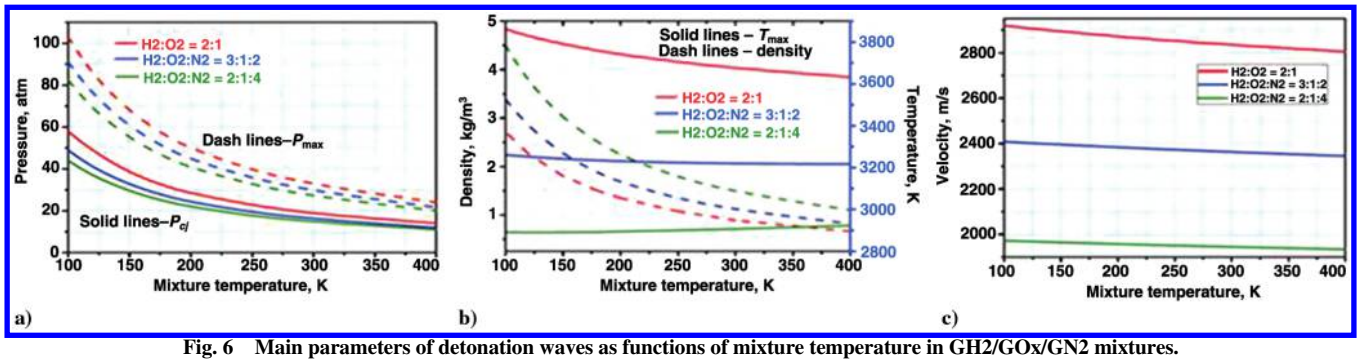

Fig. 6 Main parameters of detonation waves as functions of mixture temperature in GH2/GOx/GN2 mixtures.

wave propagating directly ahead of the combustion front. A detonation wave may be generated by a localized blast from a high explsoive charge. Recent experiments show that detonation in stoichiometric hydrogen/air mixtures enclosed in a large hemispherical envelope can be initiated by a blast of 10 g of C-4 explosive located at the center of the hemisphere [8]. The stationary detonation wave profile may be described by the Chapman–Jouguet theory extended by Zeldovich, Von Neumann and Doering (ZND) [6,9,10]. The ZND model with full chemical kinetics including 21 chemical reactions [11] was used to calculate the characteristics of the detonation waves in unconfined cryogenic GH2/GOx/GN2 mixtures for a wide range of mixture compositions and initial temperatures (Fig. 6). As expected, the velocity v_{dw} of the detonation wave strongly depends on the composition and weakly depends on the initial mixture temperature T_{mix}. Conversely, the maximum detonation pressure p_{max} depends strongly on T_{mix} and relatively weakly on the mixture composition. The closer the mixture composition to the stoichiometric H2/Ox composition (2:1) the higher the pressure in the detonation wave. The highest pressure (≈102 atm) and temperature (≈3850 K) in a detonation wave is achieved in cryogenic stoichiometric GH2/GOx mixtures (2:1) with mixture temperatures $T_{mix} \le 100$ K. Note that despite the fact that the detonation wave front is generally unstable with respect to the formation of a multidimensional cellular structure [12–14], the main parameters of real detonation waves are close to those given by the ZND theory [6,15,16]. The pressure and temperature of the detonation waves in GH2/GOx/GN2 mixtures are smaller than those in stoichiometric GH2/GOx mixtures. Nevertheless, the measured pressures in all the blast waves from the HOVI tests are an order of magnitude lower than the pressure in the detonation waves, except for HOVI test 9. Similarly, the blast wave velocity is a factor of 4 ÷ 5 smaller than the velocity of the steady detonation wave (Table 1). Thus, except in HOVI test 9, detonation was not observed in the HOVI tests.

Deflagration, as opposed to detonation, is slow subsonic combustion mediated by heat conduction whereby the hot gas behind the narrow reaction zone heats and ignites the adjacent layers of the unreacted cold gas mixture. The pressure in a deflagration wave is very close to $p_{atm} = 1$ atm. There are three main processes determining the deflagration wave speed: conductive heat transfer from the reaction zone to the cold mixture, turbulence in the wave front, and thermal expansion of hot combustion products behind the front. The laminar flame speed, which is determined by the conductive heat transfer in a quiescent gas, can be estimated as $v_D = L_D/\tau_{burn} = \sqrt{\kappa_{air} R_{burn}/C_{air}\rho_{air}} \simeq (1.5 \div 2)$ m/s where $\tau_{burn} = R_{burn}^{-1} = \tau_{H2} \simeq 3 \times 10^{-6}$ s is the typical reaction time for the GH2/GOx/GN2 mixtures. Here we took advantage of a simplified model that takes into account that in the parameter regime of interest the reaction rate is mainly limited by the initiation reactions $H_2 + O_2 \rightarrow OH + OH$ and $H_2 + O_2 \rightarrow HO_2 + H$ [17]. The rate of these reactions may be written as $R_{burn} = A(T) C_{H2} C_{Ox} \equiv C_{H2}/\tau_{burn}$ [18] where $A(T) = 5.5 \times 10^7 \exp(-19680/T) + 0.74 T^{2.43} \exp(-26926/T)$ [m³/(mol · s)] and T is in degrees Kelvin. Note that this approximation is close to the one-step mechanism of Mitani and Williams [13].

Thermal expansion of hot combustion products results in the observed flame front speed $v_{front} = v_D T_{flame}/T_{mix} < 100$ m/s for the considered cryogenic mixtures. Turbulent combustion may further accelerate the flame front several fold [19]. However, in any case the front speed is expected to stay significantly below the sound speed. Our simulations of radially symmetric laminary flames initiated by a small region of hot gas ($T_0 = 1700$ K in a 1-cm-radius ball), using the standard fluid-dynamics equations with the simplified reaction term above show that for the GH2/GOx/GN2 (nitrogen gas) (2:1:4) mixture the resulting deflagration wave is characterized by the following parameters: $p_{max} \cong 1$ atm, $T_{max} = 2500$ K, and $v_{front} = 28$ m/s. This is consistent with recent experimental studies of stoichiometric H2/Ox mixtures, which show that under normal conditions the flame front velocity is $v_{front} = 20 \div 33$ m/s and the pressure is close to 1 atm [20].

It was also found in the simulations that for different compositions and initial temperatures the pressure in the combustion wave is very close to the atmospheric pressure, and its length scale is much greater than that of temperature, in other words, the temperature wave is much more localized than the pressure wave. This is in contrast to the detonation wave where the temperature and pressure waves have the same length scale. The temperature and velocity of the steady-state deflagration wave are found to be $T_{max} = 3000$ K and $v_{front} = 30$ m/s for the stoichiometric GH2/GOx mixture, and $T_{max} = 2500$ K and $v_{front} = 28$ m/s for the GH2/GOx/GN2 mixture (2:1:4). The preceding analysis shows that deflagration waves propagating in cryogenic GH2/GOx/GN2 mixtures have pressure $p \approx p_{atm} = 1$ and front velocity $v_{front} \approx (25 \div 100)$ m/s. At the same time, according to the sensor data, in all the HOVI tests the observed pressure and front velocities exceed those of the deflagration waves by at least a factor of 3 ÷ 5 (Table 1).

B. Formation of H2/Ox Aerosols

Let us first discuss the first HOVI test group (Fig. 4, left) in which the impact of the tanks with the rupture devices results in a breach of the bottom domes in both the LH2 and the LOx tank. The turbulent LH2 jet from the breach impinges on the hot ground and breaks into droplets. The rupture of the bottom dome of the LOx tank occurs with a time delay $t_{delay} \sim (20 \div 40)$ ms for HOVI tests 13 and 14. The escaping LOx stream breaks into droplets after impact with the LH2 tank top. LOx droplets scatter from the tank surface during the time of ~50 ms from the LOx tank rupture to ignition. Note that evaporation of cryogenic liquid droplets in contact with the ground is a relatively slow process due to film boiling. Our estimates show that in the presence of film boiling (Leidenfrost effect) the time for a typical droplet to evaporate exceeds a few seconds.

Fragmentation of a liquid stream into droplets is a complex and poorly understood phenomenon. Droplet sizes may vary significantly. The typical droplet radius depends on the parameters of both the liquid and the gas [21]. Recent experimental studies of liquid jets impinging on a flat smooth surface established the following empirical correlation for the mean droplet radius [22]:

$$r_d = 2.53 \times 10^5 d_h Re^{-1.28} We^{0.4} (\mu_L/\mu_{air})^{-1.16}, \quad Re = \frac{d_h \nu_L \rho_L}{\mu_L}, \quad We = \frac{d_h \nu_L^2 \rho_L}{\sigma_L} \tag{1}$$

where μ is the dynamic viscosity with $\mu_{air} = 1.63 \times 10^{-5}$ Pa s for air, $\mu_{LH2} = 1.32 \times 10^{-5}$ Pa s for LH2, and $\mu_{LOx} = 1.96 \times 10^{-5}$ Pa s for

LOx, v_L is liquid velocity, ρ_L is the liquid density, $d_h \sim 10$ cm is the jet diameter, and σ is the surface tension. Assuming $v_L = v_0 = 30$ m/s (see Sec. II), by Eq. (1) the typical radius of the droplets in the H2 cloud is about $r_{\mathrm{dr,H2}} = 8$ mm and in the Ox cloud is about $r_{\mathrm{dr,Ox}} = 0.5$ mm. Note that these values are practically independent of the jet diameter d_h.

The typical droplets of radius r_{dr} and mass $m = 4\pi\rho_L r_{\mathrm{dr}}^3/3$ bouncing off of the ground move with initial velocity of order v_0 and fly through the air with temperature $T_{\mathrm{air}} \approx 300$ K and pressure $p_{\mathrm{air}} = 1$ atm. The droplet velocity v is slowed by air drag and is governed by:

$$m\frac{\mathrm{d}v}{\mathrm{d}t} = -\frac{C_d}{2}\rho_{\mathrm{air}} v^2 \pi r_{\mathrm{dr}}^2 \tag{2}$$

Solving this equation for the velocity and the travel distance as functions of time t yields

$$v(t) = \frac{v_0}{1 + t/\tau_v}, \quad L_v(t) = v_0\tau_v \ln\left(1 + \frac{t}{\tau_v}\right), \quad \tau_v = \frac{8\rho_L r_{\mathrm{dr}}}{3\rho_{\mathrm{air}} C_d v_0} \tag{3}$$

Assuming the drag coefficient for a droplet to be $C_d \approx 0.4$, by Eq. (3) the travel distance for HOVI tests 13 and 14 is equal to $L_v \approx 2.7$ m for the typical LH2 droplets and the explosion delay time $t \approx 90$ ms. Similarly, $L_v \approx 2.8$ m for the typical LOx droplets and the explosion delay time $t \approx 60$ ms. These values agree with the observed sizes of the H2 and Ox aerosol clouds and imply that hydrogen and oxygen droplets have time to mix.

C. Aerosol Explosion

The LH2 and LOx droplets are evaporated partly by the contact with the hot combustion products and air. Therefore, aerosol clouds containing both liquid droplets and H2, Ox, and N2 gases form in the HOVI tests. During time $\tau_d \le 100$ ms H2 and Ox clouds partly mix and the gaseous H2 and Ox mixture ignites. The temperature of such a burning mixture can reach $T_{\mathrm{flame}} = 3000$ K ÷ 3850 K (Sec. III.A). The GH2 and GOx masses increase due to droplet evaporation within the aerosols. The mechanism of droplet evaporation should be very efficient to add a significant amount of unburned reactants to the mixture during the short explosion duration of a few milliseconds to provide a significant amplifying effect. An important property of LH2 and LOx is their very low critical temperatures: $T_c = 33.2$ K for H2 and $T_c = 154.5$ K for Ox. This means that intense evaporation occurs already at relatively small droplet superheats.

A natural candidate for the primary heat-transfer mechanism is heat conduction from the hot combustion products through the gas phase [9]. Let us estimate the fraction of the droplet mass that would evaporate by heat conduction during time $\tau_d \approx 3$ ms corresponding to the typical observed duration of the pressure spike in the aerosol cloud (Table 1). If $L_D = \sqrt{\kappa_g \tau/\rho_g c_g} \approx 0.5$ mm is the thermo-diffusion length in the gas phase where $\kappa_g \simeq 0.1$ W/(m · K) is the gas thermal conductivity at ambient temperature, $\rho_g \approx 1$ kg/m^3 is the gas mass density, and $c_g \approx 10^3$ J/(kg · K) is the specific heat at constant pressure, then the heat balance $m_{\mathrm{evap}} C_L \rho_L (T_c - T_L) \approx 4\pi r_{\mathrm{dr}}^2 \tau_d \kappa_g T_{\mathrm{flame}}/L_D$, yields $m_{\mathrm{evap}} \approx 4 \times 10^{-3}$ g for an LH2 droplet of radius $r_{\mathrm{dr,H2}} = 8$ mm with mass $m_{\mathrm{dr}} = 4\pi r_{\mathrm{dr}}^3 \rho_L/3 = 0.15$ g. This estimate shows that only a small fraction (a few percent) of the droplet mass may evaporate during the short explosion time. A similar situation takes place for LOx droplets of radius $r_{\mathrm{dr,Ox}} = 0.5$ mm. This is due to the fact that in an aerosol formed as a result of a splash the droplets have rather large radii, which prevents them from being evaporated efficiently by the conductive heat-transfer mechanism.

In the case of relatively large droplet radii ($r_{\mathrm{dr}} > 0.5$ mm) thermal radiation from the hot combustion products with temperature $T >$ 3000 K to the cold droplets may be the most efficient mechanism of heat transfer. Note that the explosions in the HOVI tests were accompanied by strong flashes of bright white light similar to those observed in the detonation experiments on unconfined H2/air mixtures [8]. Heated combustion products, mainly water, will radiate in the infrared with the maximum intensity at wavelength $\lambda \approx (1 \div 3)$ μm According to the infrared absorption data in [23,24] the peak in the absorption coefficient for LH2 occurs at wavelength $\lambda_{\mathrm{absorp,LH2}} \approx 2.2$ μm, which lies within this spectral range. At that wavelength the absorption length (the inverse of the absorption coefficient: $\alpha_{\mathrm{absorp}} = l_{\mathrm{absorp}}^{-1}$) in LH2 is $l_{\mathrm{absorp,LH2}} \approx 3$ mm. Therefore, in the infrared the droplets are opaque and are able to absorb a significant portion of the incoming radiation. Furthermore, because $l_{\mathrm{absorp,LH2}}$ is comparable to the droplet radius, radiation will be absorbed in the droplet bulk, raising the temperature of the liquid phase inside without significant evaporation at the droplet surface. Thus, thermal radiation may quickly raise the LH2 and LOx droplet temperatures to the critical temperatures resulting in an explosive vaporization of the entire droplet. This greatly enhances aerosol combustion.

The evaporation time for the droplets subject to thermal radiation can be estimated via the heat balance:

$$C_L\rho_L(T_c - T_L)\left(\frac{4\pi}{3}r_{\mathrm{dr}}^3\right) \simeq \varepsilon\sigma T_{\mathrm{flame}}^4(\alpha_{\mathrm{absorp}} r_{\mathrm{dr}})4\pi r_{\mathrm{dr}}^2 \tau_{\mathrm{evap}} \tag{4}$$

where $\sigma = 5.67 \times 10^{-8}$ W/m^2/K^4 is the Stephan-Boltzmann constant and ε is the droplet emissivity. The value $\varepsilon \approx 0.3$ was estimated assuming that a significant portion of the radiation spectrum is absorbed by the droplet. Note that a more precise estimation of the absorption efficiency requires a detailed analysis of a very complex problem of infrared emission by the combustion products and propagation through a highly heterogeneous aerosol mixture, which is beyond the scope of this paper. Here semiquantitative estimates are used to capture the orders of magnitude of the quantities of interest and to fit them to the experimental data. As follows from Eq. (4)

$$\tau_{\mathrm{evap}} = \tau_1\left(\frac{T_1}{T_{\mathrm{flame}}}\right)^4, \qquad \tau_1 = \frac{C_L\rho_L(T_c - T_L)}{3\alpha_{\mathrm{absorp}}\varepsilon\sigma T_1^4} \tag{5}$$

where $T_1 = 3500$ K is the characteristic flame temperature. Note that the evaporation time does not depend on the droplet radius when $r_{\mathrm{dr}}\alpha_{\mathrm{absorp}} \ll 1$ and strongly depends on the flame temperature T_{flame}. Taking $\varepsilon\alpha_{\mathrm{absorp}} \ge 80$ m^{-1} and the droplet radii from Sec. III.B the value of $\tau_{\mathrm{evap}} \le 5$ ms for the LH2 and the LOx droplets at $T = 3500$ K. Of course, τ_{evap} depends on a number of factors and may vary from several milliseconds to tens of milliseconds.

Importantly, vaporization of the LH2 and LOx droplets results in an abrupt increase of the combustible gas density and leads to a strong buildup of pressure in the combustion products. The total mass of the burned GH2, $m_{\mathrm{H2}}^{\mathrm{burned}} = m_{\mathrm{GH2}} + m_{\mathrm{H2,drop}}$, is controlled by the available mass of GOx, $m_{\mathrm{Ox}}^{\mathrm{burned}} = m_{\mathrm{GOx}} + m_{\mathrm{Ox,drop}} = 8m_{\mathrm{Hx}}^{\mathrm{burned}}$, formed by the initial gaseous Ox and the evaporated LOx droplets mixed with GH2. The mass of the products (water) is $m_{\mathrm{H2O}} = m_{\mathrm{Ox}}^{\mathrm{burned}} + m_{\mathrm{H2}}^{\mathrm{burned}} = 9m_{\mathrm{H2}}^{\mathrm{burned}}$ and the pressure of the aerosol combustion wave can be estimated as

$$p_{\mathrm{acw}} = \left[9R_{\mathrm{H_2O}}(\rho_{\mathrm{GH2}} + \rho_{\mathrm{H2}}^{\mathrm{droplet}}) + \sum_i R_i\rho_i\right]T_{\mathrm{flame}} \tag{6}$$

where ρ_l, R are the mass density and the gas constants for the ith unburned gas component, $\rho_{\mathrm{H2}}^{\mathrm{droplet}} = m_{\mathrm{H2}}^{\mathrm{droplet}}/V_L$, where $V_L = 2\pi L^3/3$ is the volume of the hemisphere in which the aerosol cloud is mixed, and P_{acw} is the pressure in the aerosol combustion wave. Assuming P_{acw} is equal to the maximum pressure p_{max} that is determined by the sensor data (Table 1) the droplet density can be estimated from Eq. (6) as

$$\rho_{\mathrm{O2}}^{\mathrm{droplet}} = 8\rho_{\mathrm{H_2}}^{\mathrm{droplet}} = 8\left[\frac{p_{\mathrm{max}}}{9R_{\mathrm{H_2O}}T_{\mathrm{flame}}} - \rho_{\mathrm{GH2}} - \frac{\sum_i R_i\rho_i}{9R_{\mathrm{H_2O}}}\right]$$
$$\approx \frac{8p_{\mathrm{max}}}{9R_{\mathrm{H_2O}}T_{\mathrm{flame}}} \quad \text{for } p_{\mathrm{max}} \gg p_{\mathrm{atm}} = 1 \text{ atm} \tag{7}$$

Aerosol combustion was simulated using the standard equations of fluid dynamics under radial symmetry with extra terms accounting

Table 2 Main parameters of aerosol combustion and the sensor data

HOVI test	Maximum pressure from sensor data, atm	Calculated droplet mass in the mixed H2/Ox aerosol cloud, kg	Calculated blast wave velocity V_b, m/s
13	3.3 ÷ 4.2	≈0.67 LH2 ≈5.4 LOx	≈760
2	3.2 ÷ 5.4	0 LH2 3.8 LOx	≈785
5	2.5 ÷ 3	0 LH2 2.7 LOx	≈660
9 (double tanks)	80 ÷ 110	8.3 ÷ 15.2 LH2 66 ÷ 121 LOx	2500 ÷ 2928

for droplet evaporation on average. Specifically, evaporation of LH2 droplets was accounted for by adding a term $C_{H2}^{droplet}\tau_{evap}^{-1}(T/T_1)^4$ to the right-hand side of the species conservation equation for C_{H2}. Here $C_{H2}^{droplet}$ is the molar density of H2 contained in the LH2 droplets, and τ_{evap} is given by Eq. (4). A similar term is introduced in the species-conservation equation for C_{Ox}, and two extra equations are added that describe conservation of species for $C_{H2}^{droplet}$ and $C_{Ox}^{droplet}$ in the liquid phase, assuming that the liquid phase is immobile. Then, to simulate aerosol explosions in the first group of the HOVI tests, the initial values of $C_{H2}^{droplet} > 0$ and $C_{Ox}^{droplet} > 0$ were chosen so that the pressure in the aerosol combustion wave coincides with p_{max} in the explosion wave measured by the sensors (Table 2). For example, according to Eq. (7), the sensor reading of $p_{max} \approx 4.2$ atm in HOVI test 13 corresponds to an aerosol combustion wave with $C_{H2}^{droplet} = 20$ mol/m^3 ($\rho_{H2}^{droplet} = 0.04$ kg/m^3) and $C_{Ox}^{droplet} \approx 10$ mol/m^3 ($\rho_{Ox}^{droplet} = 0.32$ kg/m^3). The results for these parameters with the evaporation time $\tau_{evap} \approx 1$ ms for $T_1 = 3500$ K, the initial conditions $p_0 = 1$ atm, $T_0 = 100$ K for $r > r_0 = 1$ cm and $p_0 = 1$ atm, $T_0 = 2500$ K for $r < r_0 = 1$ cm are shown in Fig. 7. The combustion wave parameters were found to be $T_{max} = 3300$ K and $v = 600$ m/s for $p_{max} = 4.2$ atm. Note that combustion front velocity (Table 2) agrees with the one observed experimentally (Table 1).

D. Deflagration-to-Detonation Transition in Unconfined Aerosol Mixtures

Deflagration in the explosive H2/Ox mixtures may be initiated by a small spark or injection of hot gas with temperature $T > T_{ign}$. Due to the presence of aerosols the deflagration wave accelerates, and its pressure increases (see Fig. 8, where the inserts show early stages of the process). When the aerosol pressure exceeds the value $\sim p_{cj}$ a strong detonation wave may arise. The characteristics of this wave are determined only by the parameters of the H2/Ox mixture and do not depend on the initial condition triggering the explosion. Thus, aerosol H2/Ox mixtures pose the greatest explosion hazard. These mixtures are easily ignited and can produce an especially strong explosion when the mixtures are close to the stoichiometric composition. This effect happens at relatively high droplet densities of both the H2 and the Ox components or even of LOx alone. The first case is shown in Fig. 8 in which the formation of a detonation wave in the aerosol H2/Ox mixture with droplet densities $\rho_{H2}^{droplet} = 0.08$ kg/m^3 and $\rho_{Ox}^{droplet} = 0.64$ kg/m^3, the evaporation time $\tau_{evap} \approx 1$ ms and initial conditions $p_0 = 1$ atm and $T_0 = 100$ K for $r > r_0 = 1$ cm and $T_0 = 2500$ K for $r < r_0 = 1$ cm is presented.

The second case is shown in Fig. 9 where the formation of a detonation wave in the aerosol H2/Ox mixture (3:1) with the droplet densities $\rho_{H2}^{droplet} = 0$, $\rho_{Ox}^{droplet} = 0.48$ kg/m^3, $\tau_{evap} = 1$ ms and the same initial conditions is presented. The inserts in Fig. 9 show the early stage of the process. The characteristics of the steady wave are $p_{max} \cong 102$ atm, $T_{max} = 3800$ K, $v = 3000$ m/s and are close to those in Fig. 6. This result leads to an important conclusion: a strong detonation blast may be initiated by a spark or injection of hot gas in an aerosol mixture, not just by a strong shock wave, as is the case for gaseous mixtures [8]. Note that this conclusion has been confirmed in the very recent studies of detonation initiation in two-phase GH2/LOx mixtures [17]. Also note that the maximum pressure of the aerosol detonation wave can even exceed that of the detonation wave in gas mixtures.

The aerosol-detonation scenario is apparently realized in HOVI test 9, which resulted in an unusually strong blast. Note that the effect of deflagration-to-detonation transition in the preceding aerosol H2/Ox/N2 mixtures also occurs at lower rates of droplet evaporation, for example, when the evaporation time $\tau_{evap} > 1$ ms. However, for larger values of τ_{evap} higher droplet mass is necessary. For example, for stoichiometric aerosol H2/Ox mixtures one needs $\rho_{H2}^{droplet} = 0.32$ kg/m^3 at $\tau_{evap} = 5$ ms.

IV. Cavitation-Induced Ignition of H2/Ox/N2 Mixtures

One of the puzzling questions in the studies of cryogenic explosions is the mechanism of ignition in cryogenic H2/Ox/N2 mixtures. In the 1970s Farber hypothesized that the source of self-ignition in cryogenic Ox/H2 mixtures can be some sort of piezoelectric effect between the ice crystals of solid oxygen (SOx) and the colder H2 gas (GH2), or that there may be a static-charge buildup due to the transport of hydrogen bubbles [25,26]. However, his arguments meet with serious objections. Indeed, both hydrogen and oxygen, in either gas, liquid, or solid phase are formed by covalently bonded dumbbell-shaped molecules H-H and O = O, respectively. SOx, like any other molecular crystal, is built from the O = O dumbbells held together by weak van der Waals intermolecular forces. At pressures of about 1 atm and temperatures below 54 K SOx forms a molecular crystal in the γ phase with a cubic structure, and below 24 K, SOx has monoclinic crystal structure [27]. Therefore, SOx is not piezoelectric: the O = O dumbbells cannot produce piezoelectricity upon deformation because O = O molecules do not possess any dipole moment. The surface of SOx is nonpolar, either. Note that the binding energy of the dumbbell O = O molecule is equal to 5.12 eV, whereas the kinetic energy of the O = O molecule moving with a velocity of about 100 m/s is less than 2 meV. Therefore, moving O = O molecules cannot charge the solid oxygen surface.

Multiple tests, including the HOVI tests, give clear evidence that ignition in cryogenic H2/Ox mixtures is not due to external sources. GH2 released alone does not explode, despite large amount of oxygen present in the air. Ignition occurs when cryogenic hydrogen and oxygen in gaseous or aerosol form as well as liquid oxygen (LOx)

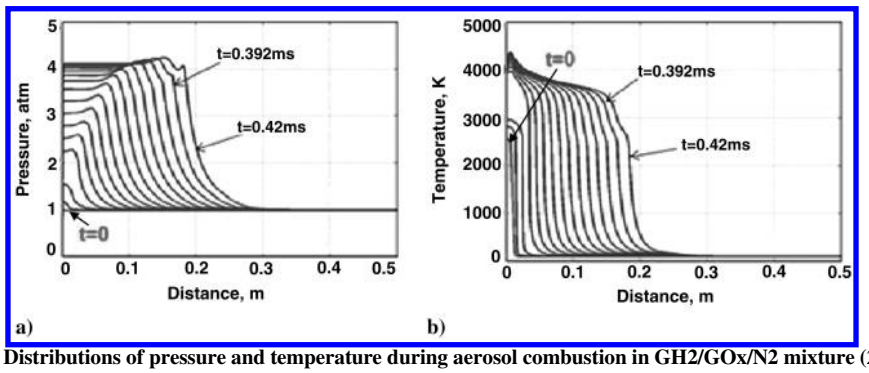

Fig. 7 Distributions of pressure and temperature during aerosol combustion in GH2/GOx/N2 mixture (2:1:4).

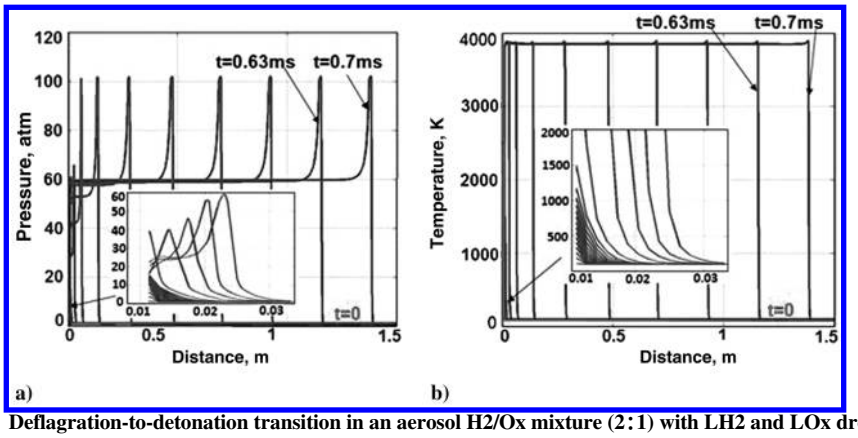

Fig. 8 Deflagration-to-detonation transition in an aerosol H2/Ox mixture (2:1) with LH2 and LOx droplets.

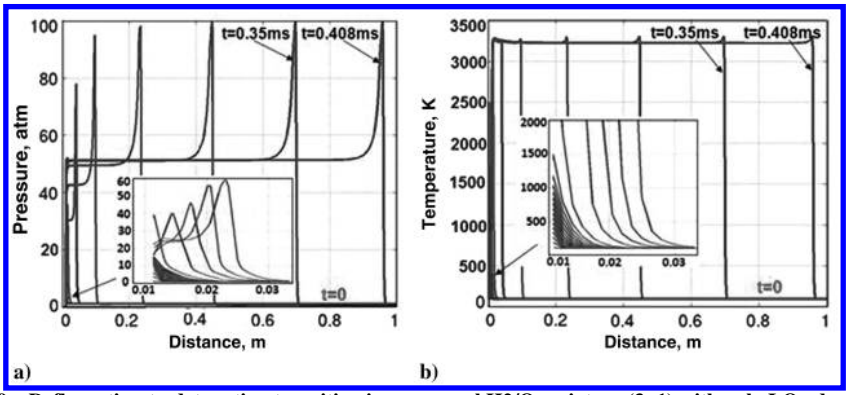

Fig. 9 Deflagration-to-detonation transition in an aerosol H2/Ox mixture (3:1) with only LOx droplets.

are available. The HOVI tests showed that self-ignition of cryogenic mixtures always occurs promptly within a short time of less than 100 ms after cryogenic H2 and Ox streams are mixed with a turbulent LOx stream. This condition is fulfilled in all HOVI tests.

A cavitation-induced mechanism that may explain self-ignition in cryogenic H2/Ox mixtures under the considered conditions was recently proposed in [28]. Cavitation refers to the formation and compression of vapor bubbles in a liquid under the action of an applied pressure jump between the liquid and the gas phases. Pure GOx vapor bubbles will inevitably form in LOx escaping from the ruptured tank because the loss of tank overpressure results in the liquid becoming supersaturated and prone to boiling. GH2-containing GOx vapor bubbles will also be created by turbulent mixing of the GH2 and GOx flows with the LOx stream. Due to the inertial motion of the liquid, this process may result in a rapidly collapsing bubble and an increase in the gas temperature and pressure inside the bubble producing a strong shock wave [29,30]. One possible scenario (scenario 1) of cavitation-induced ignition was analyzed in [28] where the pressure jump between LOx and the bubbles is assumed to arise due to a weak shock wave due to the impact of a LOx blob against a solid object, for example, the tank wall. Although such a shock cannot ignite the gas mixture directly, it can initiate a cavitational collapse of the vapor bubbles inside LOx. The simulations of [28] show that such weak shock waves can lead to bubble collapse down to radius $R_{\min} \simeq 0.1$ mm with huge pressures $p > 1000$ atm and temperatures $T > 2500$ K inside. This causes local ignition of the GOx/GH2 mixture inside the bubble. The strong secondary shock wave generated by a bubble collapsing near the LOx interface may then propagate into the gaseous H2/Ox mixture next to the LOx interface. The secondary shock wave can be sufficient to induce combustion and even detonation in cryogenic GH2/GOx mixtures [28].

Another possible scenario (scenario 2) of cavitation-induced ignition of cryogenic Ox/H2 mixtures that may explain the appearance of fireballs near the intertank section in the *Challenger* accident and the HOVI test data is discussed next. As a result of damage to the LOx and LH2 tanks LOx blobs are ejected into the intertank space. The very cold H2 gas injected from the rupture of the LH2 tank top dome chills the interfaces of these LOx blobs. One such flying blob may impact a solid surface, then another LOx blob may impact the first one (Fig. 10a). As a result, several Ox vapor bubbles with admixed GH2 and chilled interfaces may form (Fig. 10b). Note that the saturated Ox vapor pressure p_s is a rapidly decreasing function of the liquid-vapor interface temperature $p_s(T_s) =$

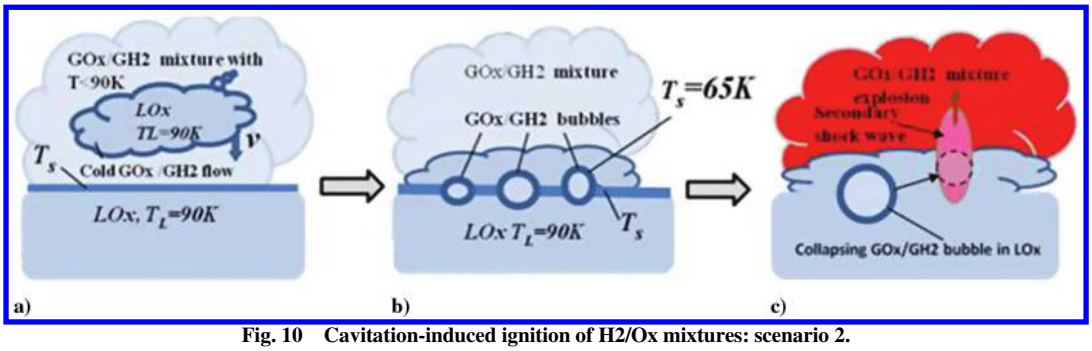

Fig. 10 Cavitation-induced ignition of H2/Ox mixtures: scenario 2.

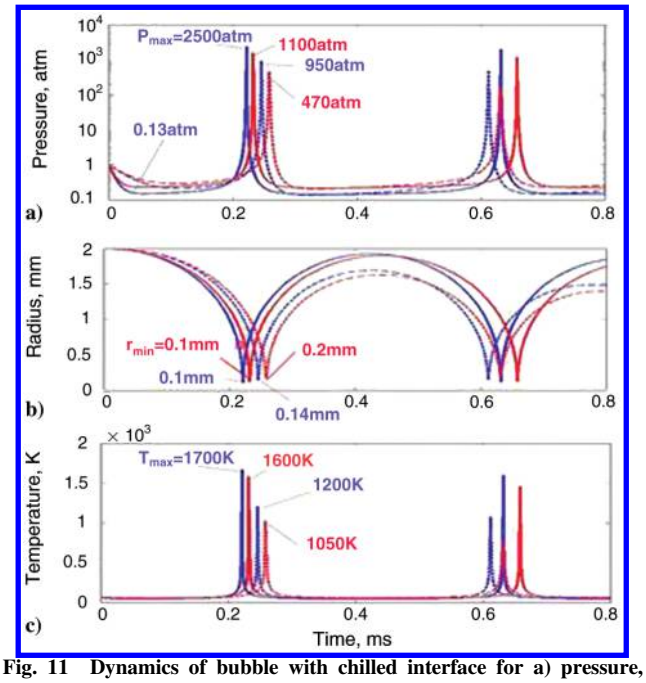

Fig. 11 Dynamics of bubble with chilled interface for a) pressure, b) radius, and c) H2/Ox temperature. Accommodation coefficient $\beta = 1$ (solid lines) and $\beta = 0.3$ (dashed lines).

$p_c(T_s/T_c)^{\lambda}$ where $\lambda = 7$, and $p_c = 50.43$ atm and $T_c = 154.58$ K are the critical pressure and temperature for Ox, respectively [31]. Therefore, the pressure inside the bubble with a chilled interface will drop very quickly to $p_s(T_s)$, while the pressure in the liquid remains equal to $p_{\text{atm}} = 1$ atm. Due to the pressure difference $(p_{\text{atm}} - p_s)$, the bubble will start to compress rapidly. Due to the inertial motion of the liquid, this process will result in bubble collapse and spiking of the gas temperature and pressure inside the bubble (Fig. 11). The presence in the bubble of even a small amount of noncondensable GH2 sharply increases the values of $p_{\max}$ and $T_{\max}$ due to local explosion of the GH2/GOx mixture inside the bubble. Simulations of the governing equations for a cavitating bubble [26] show that bubbles of initial radius ~1 mm with the surface temperature $T_s < 70$ K inside a thin surface liquid layer of ~0.1-mm thickness can compress to the radius R min ~0.1 mm. The gas temperature and pressure in such a bubble may exceed 2500 atm and 1700 K, respectively. This effect is shown in Fig. 11 where the results of simulation are presented for the initial conditions pressure $p = 1$ atm and $p_{\text{H2}} = 0.01$ atm inside the bubble, surface temperature $Ts = 65$ K (blue curves) and 70 K (red curves). The strong shock wave generated by the bubble collapsing near the LOx/GOx interface may then propagate into the gaseous H2/Ox mixture and induce combustion (Fig. 10c) and even detonation in cryogenic GH2/GOx mixtures.

Formation of detonation waves in hemispherical unconfined GH2/GOx mixtures induced by the cavitation-induced ignition via shock waves generated by the collapsing bubble near the liquid-gas interface is shown in Fig. 12. The initial mixture temperature and pressure are $T_0 = 100$ K and $p = 1$ atm, respectively, for the radius $r > 0.15$ mm and a hot compressed gas with temperature $T_0 = 1500$ K and pressure $p_0 = 350$ atm for $r < 0.15$ mm. It was found that the local jump of pressure $p \geq 200$ atm and temperature $T \geq 500$ K in a region of radius $r_0 > 0.1$ mm (collapsed bubble) is sufficient to induce detonation in the GH2/GOx mixture above the liquid surface. The obtained characteristics of the steady waves are $p_{\max} \cong 100$ atm, $p_{cj} \cong 60$ atm, $T_{\max} = 3800$ K, $v = 3000$ m/s for stoichiometric GH2/GOx mixture (Fig. 12) and $p_{\max} = 82$ atm, $p_{cj} = 45$ atm, $T_{\max} = 2800$ K, $v_{\text{dw}} = 2000$ m/s for GH2/GOx/GN2 mixture (2:1:4) are close to those in Fig. 6.

The strong shock wave generated by a bubble collapsing near the LOx interface can excite a deflagration wave in inhomogeneous unconfined H2/Ox/N2 mixtures. Indeed, such a shock wave can induce a detonation wave in a hydrogen-rich area located near the LOx surface. If this area is surrounded by a region with low H2 density then the detonation wave will rapidly dissipate there, and the temperature wave can initiate deflagration in the mixture at the other side of the hydrogen-depleted region. Numerical simulations confirmed this scenario in a strongly inhomogeneous cryogenic H2/Ox aerosol. It seems that the most likely deflagration initiation scenario is that of a bubble collapse-generated shock wave whose pressure decays inside a thin liquid layer between the strongly inhomogeneous cryogenic H2/Ox aerosol. It seems that the most likely deflagration initiation scenario is that of a bubble collapse-generated shock wave, whose pressure decays inside a thin liquid layer between the collapsed bubble and the interface. At the same time, hot gases forming after the bubble collapse may be injected into the aerosol H2/Ox mixture, igniting it. Numerical simulations confirmed feasibility of this scenario. For example, injection of hot gases from a collapsing bubble into the aerosol GH2/GOx/GN2 (2:1:4) or (3:1:2) mixtures modeled by an initial condition $T > 1500$ K and $p > 50$ atm for $r < 0.2$ mm and $T = 100$ K and $p = 1$ atm for $r > 0.2$ mm induces fast deflagration waves with the steady parameters corresponding to those of Fig. 7.

Back to the cavitation-induced ignition mechanism the main requirement for the cavitation onset is a fast jump of pressure between the liquid and the vapor bubble. This jump may be of different origins. Specifically, rarefied vapor bubbles with the internal pressure $p_{\text{int}} \ll p_{\text{atm}}$ may arise in the liquid as a result of turbulent mixing of GOx and LOx streams or liquid flow past a solid object. Such rarefied bubbles will collapse under atmospheric pressure p_{atm} (scenario 3). Yet another possible scenario (scenario 4) of cavitation-induced ignition may be due to injection of LH2 droplets into LOx or vice versa. The impact of the LH2 and LOx streams with the ground results in turbulence and fragmentation of the streams into droplets. A cold LH2 droplet (with $T = 20$ K) may be captured by a hot LOx blob ($T = 90$ K). The LH2 droplet will then evaporate in an explosive manner so that the pressure inside the bubble will quickly grow and become much greater than the pressure p_L in LOx. As a consequence the bubble radius will increase, and due to the inertial motion of the liquid, the bubble expansion will lead to the final pressure much less than p_L. Afterwards, the bubble will start collapsing, and the pressure and temperature of the GH2/GOx mixture inside the bubble can become very high, initiating a strong shock wave. These scenarios were confirmed by our preliminary numerical simulations. The maximum gas pressure and temperature attainable in the collapsed

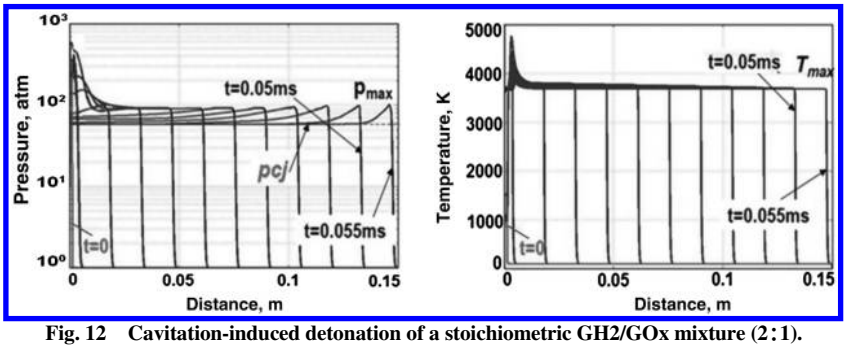

Fig. 12 Cavitation-induced detonation of a stoichiometric GH2/GOx mixture (2:1).

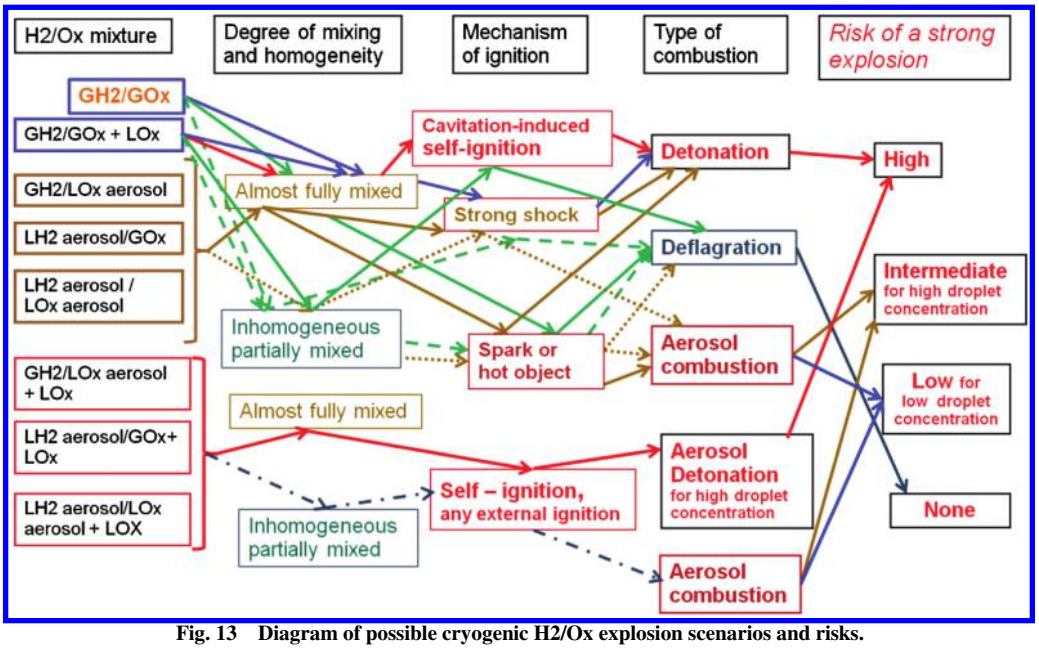

Fig. 13 Diagram of possible cryogenic H2/Ox explosion scenarios and risks.

bubbles depend on the intensity of evaporation-condensation process at bubble interface that is determined by the unknown value of the accommodation coefficient $\beta \leq 1$ in the Herz-Knudsen relation. The value of β determines the realization of a particular cavitation-induced ignition scenario described above. Scenarios 1 and 2 are more likely when β is close to 1, whereas the other scenarios are more likely when $\beta \ll 1$. It is important to point out that all the preceding scenarios may occur in the same HOVI test and could occur in a single accident.

Note that in reality ignition may be intensified due to the possibility of a local explosion inside the collapsing bubbles because of the high temperature and pressure inside. Besides generating strong shock waves, the super-hot and super-compressed O, H, and OH species may form in the collapsed bubble in the process of GOx/GH2 mixture combustion. These species may be ejected from the bubble into the space above the LOx interface and easily ignite the GH2/GOx mixture located next to this interface. This important effect may also induce fast deflagrations in unconfined aerosol mixtures. Similar events may occur in the case of common bulkhead failure [32]. The main results of the analysis, summarized in Fig. 13, describes possible scenarios and conditions of different combustion types for cryogenic hydrogen/oxygen/nitrogen mixtures.

V. Conclusions

Explosion of cryogenic hydrogen/oxygen (H2/Ox) mixtures induced by breach of cryogenic liquid-rocket-propellant tanks is characterized by the following sequence of events: rupture of the tanks, release of liquid-hydrogen (LH2) and liquid-oxygen (LOx) streams from the breached tanks, evaporation and fragmentation of these liquid streams, formation and mixing of LH2 and LOx aerosol clouds, and ignition. The power of cryogenic H2/Ox mixture explosions may be highly variable because it is determined by the characteristics of the following interrelated events involving a large degree of randomness: the velocity of the tank fall, the size of the breach, the densities of the gases and droplets in the H2 and Ox clouds, the volume of the cloud overlap, and the ignition delay time. Therefore, explosions of different intensities may occur under very similar conditions. Hydrogen-Oxygen vertical-impact (HOVI) tests showed that the rupture of cryogenic tanks with similar volumes and configurations may produce totally different explosions. The maximum overpressure Δp in 4 out of 13 HOVI tests were less than 0.3 atm, but a huge pressure spike $\Delta p \approx 100$ atm was observed in one HOVI test, whereas in all other tests Δp was of the order of several atmospheres. At the same time these distinctions were not related to the differences in the structure of the tanks, their volumes, or the rupture devices. For example, the tanks in HOVI test 13 have the greatest propellant mass (129 and 840 kg for LH2 and LOx, respectively), but the explosion power induced by the rupture of these tanks was lower than that for HOVI test 2 (37 and 189 kg, respectively) and much lower than in the case of HOVI test 9 (double tanks with total mass $33 \times 2 = 66$ and $176 \times 2 = 352$ kg in the LH2 and LOx tank, respectively).

As follows from our analysis of the HOVI test data and the considered cavitation-induced ignition mechanism self-ignition of cryogenic mixtures always occurs promptly within a short time, less than 30 ms, after cryogenic H2 and Ox streams are mixed with a turbulent LOx stream. The considered aerosol combustion scenario is important for understanding the explosion conditions and risks for cryogenic hydrogen/oxygen fuels used in liquid rockets and other vehicles. The aerosol combustion intensity is determined by the H2 and Ox masses inside the overlapping area of the H2 and Ox aerosol clouds. The combustion type is determined by the composition of the mixtures, the degree of their mixing, and the ignition mechanism. A strong explosion (detonation) can arise in gaseous hydrogen/oxygen/nitrogen mixtures when they are well mixed and the ignition is induced by a strong shock. The closer the mixture is to the stoichiometric composition the stronger is the resulting detonation. Any other ignition sources, for example, by a spark or a hot object, results in slow combustion (deflagration) of gaseous cryogenic hydrogen/oxygen/nitrogen mixtures.

Self-ignition occurs when hydrogen/oxygen/nitrogen streams mix with a strong liquid-oxygen stream. Any mechanism of ignition of partially mixed aerosol hydrogen/oxygen mixtures with relatively low droplet concentrations leads to aerosol combustion, accelerated deflagration, and is characterized by the overpressure of several atmospheres. Well-mixed hydrogen/oxygen aerosol mixtures with high droplet concentrations are the most dangerous: any ignition mechanism, including self-ignition, in contact with relatively large liquid-oxygen fragments results in a strong explosion. The maximum pressure in such an explosion may exceed 100 atm for the mixtures close to stoichiometric composition.

The explosive power depends on the pressure and the size of the region of mixed hydrogen and oxygen aerosol clouds. A strong detonation may arise when the mixture is well mixed inside a large enough volume, which is determined by the ignition delay time. On the other hand, a relatively small value of $t_{\text{delay}} < 20$ ms in the HOVI tests corresponds to the case when the breaches occur in the intertank area and cryogenic hydrogen and oxygen are injected into the intertank area from the upper dome of the ruptured liquid-hydrogen tank and the lower dome of the ruptured liquid-oxygen tank. This

situation appears to have happened in the *Challenger* disaster. It was also recreated purposely in the second group of the HOVI tests. The escaped cryogenic hydrogen and oxygen streams very quickly mix together in a reletively small region and self-ignite resulting in a relatively weak blast.

Aerosol combustion accelerates deflagration and is likely to arise in the cases with maximum blast pressure from one to several atmospheres. Here, the risk of a strong explosion is intermediate. Different situations may occur when the bottom domes of both tanks are ruptured as can be seen from the first group of the HOVI tests. Here the delay can be longer due to a much larger distance separating the initial hydrogen and oxygen aerosol clouds. Such an event probably happened in HOVI test 9. This test used double tanks with the rupture devices placed underneath each tank. Following the rupture of the hydrogen tank its thermal insulation detached and shielded the hydrogen aerosol cloud from direct contact with the turbulent liquid-oxygen stream. This resulted in a longer delay time, $t_{\text{delay}} \approx 200$ ms, between the rupture and ignition. During this time the expanding hydrogen and oxygen aerosol clouds had a chance to form and mix together. As a consequence a nearly stoichiometric hydrogen/oxygen mixture confined to a hemisphere of radius of about 4 m was formed. The self-ignition of this mixture induced the strongest explosion (aerosol detonation) characterized by the maximum pressure exceeding 100 atm and the duration of about 1 ms. This strong explosion is attributed to a chance occurrence of the complex breaking dynamics of the insulating foam detaching from the double LH2 tank. Such a strong explosion was not observed in any other test, including HOVI test 10, which had the same double tanks as HOVI test 9. In the case of HOVI test 10 the value of t_{delay} was small and $p_{\max} = 1.36$ atm.

An event in which the content of the hydrogen and oxygen tanks is scattered over a relatively large area is probably the most dangerous from the point of view of the risk of the strongest explosion. Indeed, in this case the escaped hydrogen and oxygen liquids will have a long enough time to evaporate and to generate gaseous hydrogen and oxygen aerosol clouds that will have time to mix together into a large enough area before self-igniting upon contact with the ejected turbulent liquid oxygen stream. As was already noted self-ignition of cryogenic H2/Ox mixtures is always realized when cryogenic hydrogen and oxygen streams are mixed with a strong turbulent liquid-oxygen stream. At the same time the H2/Ox masses determining the explosion power of the cryogenic mixture are much smaller than the masses released from the tanks and several orders of magnitude smaller than the total LH2 and LOx masses in the tanks.

Acknowledgments

We acknowledge Frank Benz from NASA Johnson Space Center White Sands Test Facility for providing the test data for Hydrogen-Oxygen vertical impact tests performed at the facility and for valuable discussions. The work of CBM was supported by NASA via grant number NNX10AC65G.

References

[1] Cole, M. D., *Challenger: America's Space Tragedy*, Enslow Publishers, Springfield, NJ, 1995, pp. 1–48.

[2] Diane, V., *The Challenger Launch Decision: Risky Culture, Technology, and Deviance at NASA*, Univ. of Chicago Press, Chicago, 1996, pp. 1–551.

[3] *Report of the Presidential Commission on the Space Shuttle Challenger Accident*, DIANE Publishing, 1986, http://history.nasa.gov/rogersrep/genindex.htm [retrieved 4 April 2013].

[4] Lambert, R. R., "Liquid Propellant Blast Yields For Delta IV Heavy Vehicles," *34th Department of Defense Explosives Safety Board Seminar*, National Technical Information Service, ADA532286, July 2010.

[5] Gayle, J. B., Blakewood, C. H., Bransford, J. W., Swindell, W. H., and High, R. W., "Preliminary Investigation of Blast Hazards of RP-I/LOx and LH2/LOx Propellant Combinations," NASA TM-X-53240, 1965.

[6] Glassman, I., and Yetter, R. A., *Combustion*, 4th ed., Elsevier, New York, 2008, Chap. 3.

[7] Bunker, R., Eck, M., Taylor, J. W., Hancock, S., Carden, A., and LaRue, B., "Correlation of Liquid Propellants," NASA Headquarters Research and Technology Operating Plan No. WSTF-TR-0985-001-01-02, Lyndon B. Johnson Space Center, Las Cruses, NM, 2003.

[8] Groethe, M., Merilo, E., Colton, J., Chiba, S., Sato, Y., and Iwabuchi, H., "Large-Scale Hydrogen Deflagration and Detonation," *International Journal of Hydrogen Energy*, Vol. 32, No. 13, 2007, pp. 2125–2133. doi:10.1016/j.ijhydene.2007.04.016

[9] Williams, F. A., *Combustion Theory*, 2nd ed., Addison Wesley Longman, Reading, MA, 1985, Chaps. 3, 6.

[10] Zeldovich, Y. B., Barenblatt, G. I., Librovich, V. B., and Makhviladze, G. M., *The Mathematical Theory of Combustion and Explosion*, Consultants Bureau, New York, 1985, Chap. 6.

[11] Kao, S., and Shepherd, J. E., "Numerical Solution Methods for Control Volume Explosions and ZND Detonation Structure," GALCIT, Aeronautics and Mechanical Engineering, California Inst. of Technology, Rept. FM2006.007, Pasadena, 2006, http://www.galcit.caltech.edu/EDL/ [retrieved 4 April 2013].

[12] Nikolaev, Y. A., Vasil'ev, A. A., and Ul'yanitskii, B. Y., "Gas Detonation and its Application in Engineering and Technologies (Review)," *Combustion, Explosion, and Shock Waves*, Vol. 39, No. 4, 2003, pp. 382–410. doi:10.1023/A:1024726619703

[13] Mitani, T., and Williams, F. A., "Studies of Cellular Flames in Hydrogen–Oxygen–Nitrogen Mixtures," *Combustion and Flame*, Vol. 39, No. 2, 1980, pp. 169–190. doi:10.1016/0010-2180(80)90015-2

[14] Gavrikov, A. I., Efimenko, A. A., and Dorofeev, S. B., "A Model for Detonation Cell Size Prediction from Chemical Kinetics," *Combustion and Flame*, Vol. 120, No. 1, 2000, pp. 19–33. doi:10.1016/S0010-2180(99)00076-0

[15] Plaster, M., McClenagan, R. D., Benz, F. J., Shepherd, J. E., and Lee, J. H. S., "Detonation of Cryogenic Gaseous Hydrogen-Oxygen Mixtures," *Progress in Astronautics and Aeronautics*, Vol. 133, No. 1, 1991, pp. 37–55.

[16] Ripley, D. L., and Gardiner, W. C. Jr., "Shock Tube Study of the Hydrogen-Oxygen Reaction. II. Role of Exchange Initiation," *Journal of Chemical Physics*, Vol. 44, No. 6, 1966, pp. 2285. doi:10.1063/1.1727036

[17] Jouot, F., Dupre, G., Quilgars, A., Gokalp, I., and Cliquet, E., "Experimental Study of Detonation in a Cryogenic Two-Phase H2-Ox Flow," *Proceedings of the Combustion Institute*, Vol. 33, No. 2, 2011, pp. 2235–2241. doi:10.1016/j.proci.2010.06.160

[18] Michael, J. V., Sutherland, J. W., Harding, L. B., and Wagner, A. F., "Initiation in H_2/Ox: Rate Constants for $H_2 + Ox \rightarrow H + HOx$ at High Temperature," *Proceedings of the Combustion Institute*, Vol. 28, No. 2, 2000, pp. 1471–1478. doi:10.1016/S0082-0784(00)80543-3

[19] Molkov, V., Makarov, D., and Schneider, H., "LES Modelling of an Unconfined Large-Scale Hydrogen–Air Deflagration," *Journal of Physics D: Applied Physics*, Vol. 39, No. 20, 2006, pp. 4366–4376. doi:10.1088/0022-3727/39/20/012

[20] Merilo, E. G., and Groethe, M. A., "Deflagration Safety Study of Mixtures of Hydrogen and Natural Gas in a Semi-Open Space," *Proceedings of the International Conference on Hydrogen Safety*, San Sebastian, Spain, June 2007.

[21] Xu, L., Zhang, W. W., and Nagel, S. R., "Drop Splashing on a Dry Smooth Surface," *Physical Review Letters*, Vol. 94, No. 18, 2005, Paper 184505. doi:10.1103/PhysRevLett.94.184505

[22] Ahmed, M., Ashgriz, N., and Tran, H. N., "Influence of Breakup Regimes on the Droplet Size Produced by Splash-Plate Nozzles," *AIAA Journal*, Vol. 47, No. 3, 2009, pp. 516–522. doi:10.2514/1.36081

[23] Allin, E. J., Hare, W. F. J., and MacDonald, R. E., "Infrared Absorption of Liquid and Solid Hydrogen," *Physical Review*, Vol. 98, No. 2, 1955, pp. 554–555. doi:10.1103/PhysRev.98.554

[24] Allin, E. J., Gush, H. P., Hare, W. F. J., and Welsh, H. L., "The Infrared Spectrum of Liquid and Solid Hydrogen," *Del Nuovo Cimento*, Vol. 9, No. 1, 1958, pp. 77–83. doi:10.1007/BF02824231

[25] Farber, E. A., "Explosive Yield Limiting Self-Ignition Phenomena in LOx/LH2 and LOx/RP-1 Mixtures," *15 Explosives Safety Seminar*, Information for Defense Community, 18–20 Sept. 1973, pp. 1287–1303.

[26] Farber, E. A., "Prediction of Explosive Yields and Other Characteristic of Liquid Rocket Propellants," NASA, Final Rept. 10-1255, 1975.

[27] Freiman, Y. A., and Jodl, H. J., "Solid Oxygen," *Physics Reports*, Vol. 401, No. 1, 2004, pp. 1–228. doi:10.1016/j.physrep.2004.06.002

[28] Osipov, V. V., Muratov, C. B., Ponizovskaya-Devine, E., Foygel, M., and Smelyanskiy, V. N., "Cavitation-Induced Ignition Mechanisms in Cryogenic Hydrogen/Oxygen Mixtures," *Applied Physics Letters*, Vol. 98, No. 13, 2011, p. 134102. doi:10.1063/1.3571445

[29] Brennen, C. E., *Cavitation and Bubble Dynamics*, Oxford Univ. Press, Oxford, England, U.K., 1995, Chap. 3.

[30] Fujikawa, S., and Akamatsu, T., "Effects of the Nonequilibrium Condensation of Vapor on the Pressure Wave Produced by the Collapse of the Bubble in a Liquid," *Journal of Fluid Mechanics*, Vol. 97, No. 3, 1980, pp. 481–512. doi:10.1017/S0022112080002662

[31] Clark, J. A., "Universal Equations for Saturation Vapor Pressure," *40th AIAA/American Society of Mechanical Engineers/Society of Automotive Engineers/American Society for Engineering Education Joint Propulsion Conference and Exhibit*, Curran Associates Incorp., Paper 2004-4088, 2004, pp. 04-4050–04-4099.

[32] Sachdev, J. S., Hosangadi, A., Madavan, N. K., and Lawrence, S. L., "Simulations for Assessing Potential Impact of Ares I Propellant Tank Common Bulkhead Failure," *45th AIAA/American Society of Mechanical Engineers/Society of Automotive Engineers/American Society for Engineering Education Joint Propulsion Conference & Exhibit*, Curran Associates Incorp., Paper 2009-5150, 2009.

A. Ketsdever
Associate Editor